# INFLUENCE OF OBSTACLE ASPECT RATIO ON TRIPPED CYLINDER WAKES

**Tiago B. Araugo, Christophe Sicot, Jacques Boree**
Institut Pprime, UPR CNRS 3346
ENSMA, Université de Poitiers
BP 40109, France
tiago_physics@yahoo.com.br christophe.sicot@lea.ensma.fr jacques.boree@lea.ensma.fr

**Robert J. Martinuzzi**
Department of Mechanical and Manufacturing Engineering
Schulich School of Engineering, University of Calgary
2500 University Drive NW, Calgary, Alberta, Canada T2N 1N4
rmartinu@ucalgary.ca

## ABSTRACT

The influence of an asymmetrically mounted, single tripwire on the shedding and wake characteristics of a vertical, surface-mounted finite circular cylinder is investigated experimentally. Height-to-diameter aspect ratios of 3 and 6 are considered. It is shown that a critical position for the tripwire exists, which is characterised in an abrupt change in the shedding frequency and wake structure. Results further suggest that the tripwire can strengthen 2D wake properties. The influence of the aspect ratio is due to tip-wake flow interactions and thus differs fundamentally from two-dimensional geometries.

## INTRODUCTION

The presence of surface protrusions on cylindrical, nominally two-dimensional, bodies placed in a uniform flow are known to modify vortex shedding and wake dynamics, which has important implications for structural loading and flow control. For sub-critical, turbulent wake flows several studies have addressed the influence of the size and location of two symmetrically placed protrusions, typically tripwires. These wires considerable effect on the wake when placed on the cylinder at azimuthal angles, $\alpha$, ranging from 20° to 70° (cf. Igarashi, 1986; Alam et al., 2010).

Single tripwires have also been shown to impact significantly the shedding process. In particular, it has been shown that a change in shedding structure occurs about a critical angle of $50° < \alpha_c < 60°$ (Nebres & Batill, 1993; Ekmekci and Rockwell, 2011). However, most studies focus on two-dimensional geometries and thus the impact of the tip flow on the effect of surface protrusions remains poorly investigated. This effect is nevertheless important for most practical applications involving low lying structures or compact heat exchangers, where height-to-diameter aspect ratios range from 1 to 20.

## EXPERIMENTAL

The experimental set-up and nomenclature are shown schematically in Fig. 1. Circular cylinders of diameter D = 40mm and heights H = 120mm and 240mm, yielding aspect ratios of AR = H/D = 3 and 6, respectively, were mounted on a flat plate. Detailed measurements were conducted at a free stream velocity of U = 20m/s, corresponding to a Reynolds number, based on D, of $Re \approx 5\times10^4$. With the obstacle removed, the thickness of the zero-gradient, turbulent boundary layer developing on the plate is approximately 0.2D. Single tripwires of diameter d/D=0.02 were mounted on one side of the obstacle at azimuthal angles $\alpha$, from the windward stagnation point. The shedding frequency, $f_s$, was associated with the peak of the spectral density function determined from the time traces of fluctuating surface pressure and velocity measurements at x=3.5D downstream and $y \pm 1$D.

Pressure measurements were acquired along the ground plate using off-set pressure sensors having a bandwidth of [0Hz, 1.6 kHz] and a pressure range of 250 Pa (Ruiz et al, 2009). Particle Image Velocimetry (Planar PIV Lavision, software ver 7 – sensor resolution of 1376×1040 pixels$^2$) was used to acquire two velocity components along several vertical and horizontal planes. The PIV images were post-processed with a multipass algorithm with final interrogation windows of 16×16 pixels$^2$ and 50% of overlapping. Averaged PIV mean and first moment data are based on at least 1000 statistically independent image pairs. Additional hot-wire anemometry (HWA) measurements were conducted at selected locations. The HWA were single-wire, 5μm Pt-T proves using DANTEC bridges and an in-house acquisition system.

Visualisations of the mean surface flow patterns on the plate and cylinder surfaces were obtained using a mixture of oleic acid, white spirit and white kaolin particles. The plate and cylinder surfaces were painted black for contrast. The mixture is particularly well-suited for visualisations on vertical surfaces.

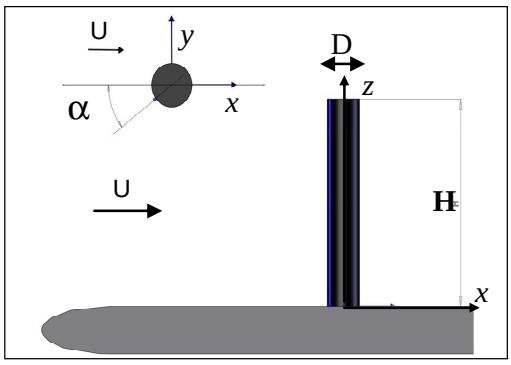


Figure 1. Schematic of experimental set-up and nomenclature.

## RESULTS

The influence of the flow field and shedding characteristics of a single tripwire along the entire height of vertical, surface-mounted cylinders is documented and discussed. Velocimetry and surface pressure fluctuation data are presented, complemented by mean surface flow visualizations for obstacles aspect rations, AR, of 3 and 6 for several tripwire positions, $\alpha$, measured from the windward stagnation point.

The tripwire influence on the shedding process is evidenced from the change in the shedding frequency, $f_s$, expressed as the Strouhal number $St = f_s D/U$ in Fig. 2 as a function of the tripwire location for AR = 3 and 6. The data for the two-dimensional (2D) case immersed in a uniform stream of Ekmekci and Rockwell (2011) is included for comparison. An abrupt reduction of $St$ occurs at a critical tripwire position in the range $55° < \alpha_c < 60°$ for all cases considered. However, the influence of the aspect ratio on the shedding behaviour is not monotonic. Firstly, the change of $St$ across the critical range is greater for AR = 6 and less for AR = 3 than for the 2D case. Upon closer inspection, $St$ for post-critical angles ($>\alpha_c$) matches, within experimental uncertainty, values for the bare (un-tripped) obstacle, whereas for the 2D case $f_s$ is higher for the bare cylinder. Unlike the 2D case, no loss of spectral intensity at the shedding frequency for $\alpha = \alpha_c$ is observed for the finite geometry.

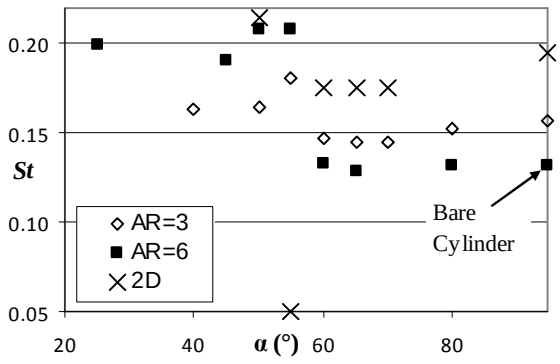


Figure 2. Shedding frequency, $St$, as a function of $\alpha$.

The influence of the obstacle aspect ratio on the shedding behaviour can be seen from the surface pressure fluctuation characteristics along the ground plate in the cylinder wake. The root-mean-square (*rms*) surface pressure distribution, in terms of the coefficient Cp', is shown in Fig. 3 along $y/D = -1$ (wire side) and = 1 (unperturbed side) for AR = 6. Generally, Cp' for $\alpha = 60°$ ($>\alpha_c$) are slightly greater than for the bare obstacle, while a strong attenuation is observed for $\alpha = 55°$ ($<\alpha_c$) and the peak occurs further upstream than for the other cases, which will be shown later to correspond to a shorter mean recirculation length. Results are similar for AR = 3.

Changes in Cp' levels may be attributed to different mechanisms. Figure 4 shows sample spectral density functions, *psdf*, of the pressure fluctuations at $x/D = 3.5$ on the wire side ($y/D = -1$). Similar behaviour is seen on the wire side. For $\alpha = 60°$ ($>\alpha_c$), and AR = 6, the *psdf* indicates that the increase in fluctuation levels, when compared to the bare case, is due to an increase in the energy content over a broad band across the spectrum. For AR = 3, while the fluctuation levels change little, the spectral peak is sharper, suggesting a more coherent motion (greater fluctuation energy concentration at $f_s$, $\alpha = 60°$). For $\alpha = 55°$ ($<\alpha_c$), the *psdf* for AR = 3 shows significant spectral broadening and decreased energy levels at $f_s$, which suggests a disruption or weaker strength of shed vortices. In contrast for AR = 6, the *psdf* shows a well-defined, sharp peak even though the fluctuation levels are much lower than for other cases. Thus, unlike the case for AR = 3, for AR = 6 a "tuning" of the shedding process appears to have occurred.

Moreover, preliminary HWA traverses in the obstacle wake indicate that the extent of the tip (free-end) effects is also influenced by the tripwire location. For example, $f_s$ is increasingly difficult to discern above a critical height from the base plate, ranging from $z = 0.3H$ ($\alpha = 55°$, AR = 3) to $z = 0.8H$ ($\alpha > 60°$, AR = 6). It is thus likely that the state of the boundary layer on the obstacle surface affects both the vortex formation process and the wake structure.

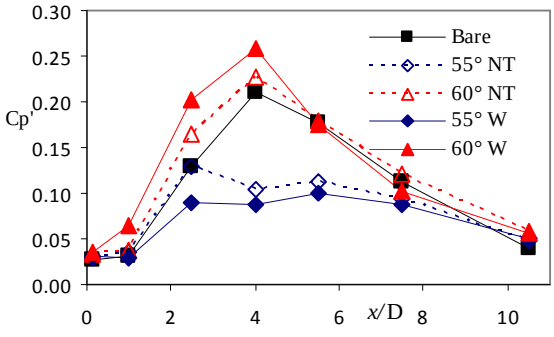


Figure 3. Cp' wake distribution along the plate: NT – unperturbed $y/D = 1$; W – wire side $y/D = -1$

Visualisations of the mean surface flow patterns provide a preliminary characterisation of the influence of the tripwire

location, $\alpha$, on the boundary layer state over the cylinder sides and the mean wake structure. Figure 5 shows an example of the mean surface flow patterns for AR = 3, $\alpha = 50°$. On the unperturbed side, the flow separates at $\theta_{so}$. The separation line varies negligibly along the height except close to the obstacle extremities. On the wire (tripped) side, the boundary layer initially separates directly upstream of the tripwire and reattaches in its lee at $\theta_c$, and finally separates at $\theta_s$. Although the influence of the free-end extends further than on the unperturbed side, $\theta_c$ and $\theta_s$.change negligibly over most of the obstacle height.

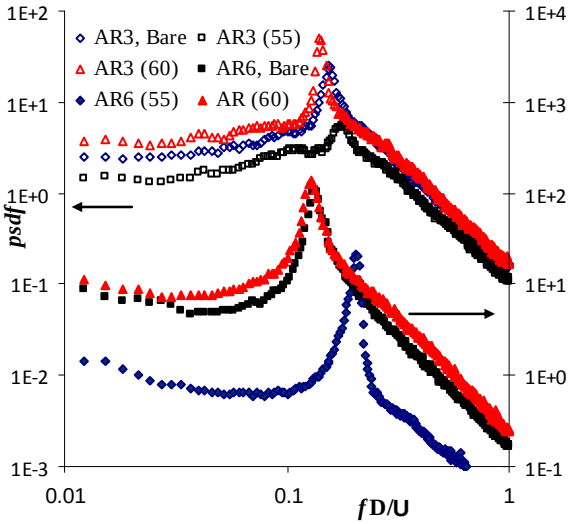


Figure 4. Frequency spectra (*psdf*) of surface pressure fluctuations at $x$ = 4D along $y$/D = -1 (wire side)

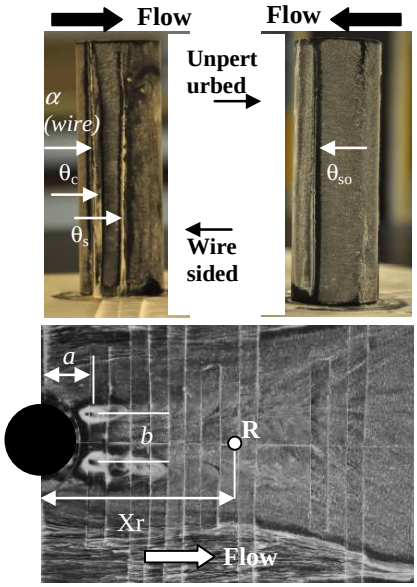


Figure 5. Surface flow visualisation for AR = 3, $\alpha = 50°$

Changes of the mean wake structure due to the tripwire location $\alpha$ can be characterised by the recirculation length and the location of the nodes associated with the footprint of the lee base vortices. The maximum recirculation length, Xr, is given by the location relative to the cylinder centre of the attachment point, **R**. The topological nature of this point changes according to tripwire location. For the bare cylinder and the case AR = 3 $\alpha = 55°$ ($< \alpha_c$), **R** is a node, while for $\alpha_c < \alpha < \sim 70°$ it is a saddle point. This difference is important as a saddle point implies the existence of a converging (negative) bifurcation line in the velocity for the plane y = 0 and thus differences in the near-plate flow.

The recirculation length, Xr, is shown in Fig. 6a. A minimum in Xr occurs for $\alpha \approx 45\pm2°$ and $\alpha \approx 50\pm2°$ for AR = 6 and 3, respectively, which is less than the critical location $\alpha_c \approx 57\pm2°$. For $\alpha > \alpha_c$, Xr changes little and approaches the value of the bare cylinders. The location of the base region reciculation nodes (foci) *a*, and their separation, *b*, as functions of $\alpha$ are shown in Fig. 6a. For AR = 6, *b* reaches a minimum at the same location as Xr ($\alpha \approx 45\pm2°$), at which

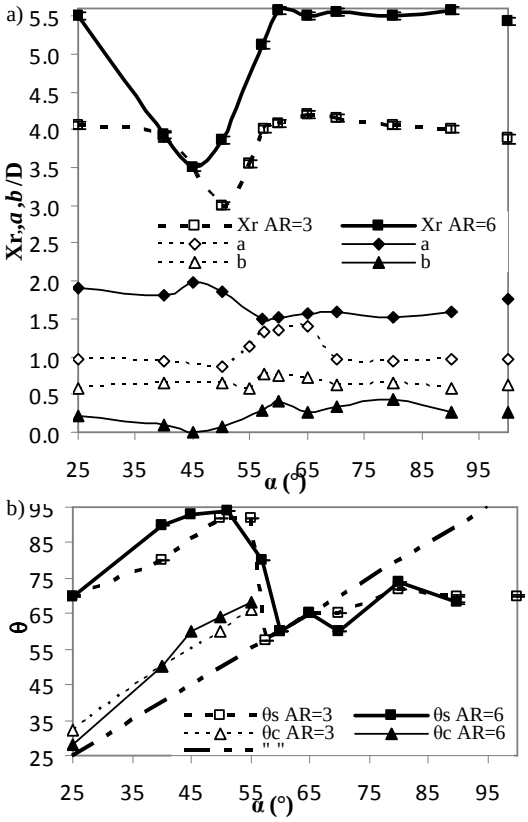


Figure 6. Summary of the surface flow visualisation results as functions of the trip wire location $\alpha$: a) Attachment length, Xr, node location, *a*, and separation *b*; b) reattachment, $\theta_c$, and separation, $\theta_s$, points on cylinder perturbed side. Values in right margin for bare cylinder.

location the nodes are difficult to distinguish. The separation increases until $\alpha \approx \alpha_c$. For AR = 3, the trend for *b* is similar, albeit the changes are less pronounced. The distance of the foci, *a*, for AR = 6 decreases abruptly at $\alpha \approx \alpha_c$. For AR = 3, the changes are more complex as *a*, in contrast to AR = 6, initially increases around the critical tripwire location, decreases for $65° < \alpha < 70°$ and changes little for larger $\alpha$ In general, for $\alpha > 70°$, Xr, *a*, *b* and *St* match those values for the bare cylinder suggesting that the flow is independent of the tripwire location. For smaller $\alpha$, however, the behaviour is more complex and aspect ratio dependent.

The changes in the mean wake structure and shedding frequency are expected to be related to the state of the boundary layer on the cylinder surface. Figure 6b shows changes as a function of $\alpha$ of the wire side reattachment, $\theta_c$, and separation point, $\theta_s$, as obtained from the flow visualisations. On the unperturbed side, the location of the boundary layer separation appears unaffected by $\alpha$ and occurs at $\theta_{so} \approx 70°$ for both geometries. On the wire side, for $\alpha < 25°$ flow separation could not be deduced from the pigment accumulation, suggesting that the flow attaches immediately in the tripwire lee. For larger $\alpha$, the boundary layer separates immediately upstream of the tripwire and reattaches downstream. For AR = 6, the reattachment point occurs increasingly downstream of the tripwire for $25° < \alpha < 45°$. For $45° < \alpha < \alpha_c$, the boundary layer reattachment length changes little and occurs at $\theta_c = \alpha + 14° \pm 2°$. For AR = 3, the reattachment length increases until $\alpha \approx 40°$ and remains thereafter constant until $\alpha_c$ at $\theta_c = \alpha + 10° \pm 2°$. For $\alpha > \alpha_c$, the boundary layer does not reattach. The behaviour of the final boundary layer separation point, $\theta_s$, is more complex. For $\alpha < 25°$, the flow separates at the value of the bare cylinder ($\theta_s \approx 70°$). As $\alpha$ increases, $\theta_s$ increases to $92° \pm 2°$ until $\alpha \approx \alpha_c$. For $\alpha_c \leq \alpha < \sim 70°$, the flow separates at the wire location ($\theta_s = \alpha$). For $\alpha = 70°$, the boundary layer separates upstream of the tripwire ($\theta_s < \alpha$), while for $\alpha > 70°$, the flow separates again at $\theta_s \approx 70° \pm 2°$.

The impact of the tripwire on the mean wake structure is significant. Figure 7 shows the sectional streamlines and contours of the *rms* vertical velocity fluctuations, w', in the plane $y = 0$ of the AR = 6 obstacle for $\alpha = 55°$ and 60°. For $\alpha = 60°$, the flow patterns are very similar to those for the bare cylinder (not shown for brevity). A recirculation node, **N**, is observed at the lee of the free-end. The streamline separating the recirculation zone gradually slopes to the wake bifurcation saddle, **Sb**. This bifurcation point implies that the flow over the base plate moves towards the line $y = 0$, resulting in **R** being a saddle point. The region of higher w' concentration roughly follows the trajectory of the separated shear layer. Downstream of the separating streamline, the downwash ($w < 0$) remains significant above the bifurcation line extending from **Sb**. In contrast, for $\alpha = 55°$ the separating streamline drops almost vertically (see $z/H < 0.5H$, $x \sim 2.8D$) and the wake downwash is much less.

Within the mean recirculation region, for $\alpha = 60°$ the flow along the back face of the cylinder above the half-saddle **S'** ($z \sim 0.2H$ in Fig. 7b) moves upwards towards the free-end. In contrast, for $\alpha = 55°$, the flow moves downwards over much of the back face (**S'** at $z \sim 0.8H$ in Fig. 7a). The location of maximum w' is of dynamic significance and changes little despite large changes in Xr. In contrast to $\alpha = 60°$, for $\alpha = 55°$ the length of the vortex formation region varies little in the vertical direction. Along the vertical bifurcation line connecting to **Sb**, $\partial w/\partial z$ is significantly smaller and the downwash in the wake is significantly reduced over much of the obstacle height (streamlines are nearly parallel to the base plate) when compared to the case $\alpha = 60°$. The vortex formation process appears more two dimensional than for $\alpha > \alpha_c$, which is consistent with a "tuning" of the shedding frequency and reduction of the incoherent contribution to the fluctuating field observed from spectra in Fig. 4.

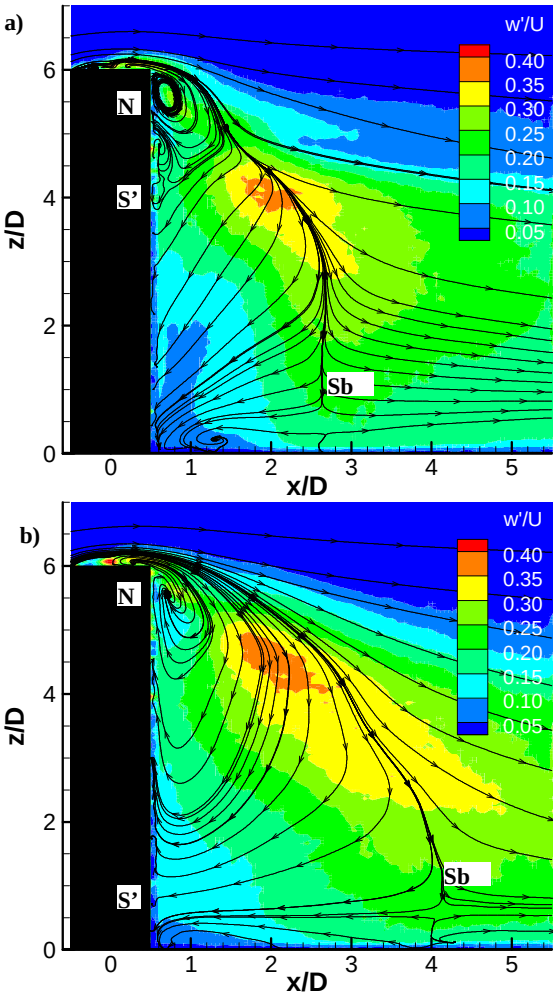


Figure 7. Sectional streamlines and w' iso-contours in plane $y = 0$ for AR = 6: a) $\alpha = 55°$; b) $\alpha = 60°$.

An overlay of the sectional streamlines and v'-iso-contours is shown in Fig. 8 for $\alpha = 55°$ and 60° for the horizontal plane $z/H = 0.3$. A more slender wake and shorter recirculation is observed for $\alpha = 55°$ than for 60° (or the bare cylinder) implied by changes in Xr or delayed separation (Fig.

6). Note that the wake flow shows only a slight asymmetry for $\alpha = 55°$, despite a significant difference in the separation point on the two sides of the cylinder (Fig. 6b). More significantly, the fluctuation levels are comparable on both tripped and unperturbed sides, despite very different separation histories on the cylinder surface.

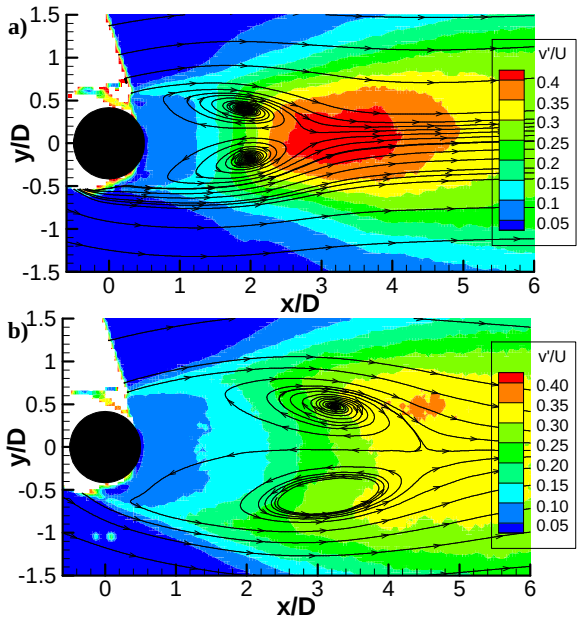


Figure 8. Sectional streamlines and v' iso-contours in plane $z = 0.3H$ for AR = 6: a) $\alpha = 55°$; b) $\alpha = 60°$.

Closer consideration is given to the influence of $\alpha$ on the separated shear layer directly behind the cylinder. The lateral profiles of the streamwise velocity, u, and the *rms* of its fluctuations, u', on the tripped side of the cylinder at $x/D = 0.5$, $z/H = 0.25$ for AR = 6 are shown in Fig. 9. For $\alpha < 30°$ or $\alpha > 65°$ the u and u' profiles are very similar to those for the bare cylinders. In the range of reduced Xr ($30° < \alpha < \alpha_c$), the profiles are shifted closer to the cylinder. The flow reattaches downstream of the tripwire and separation is delayed on the wire side. When the separation occurs at the tripwire, $\alpha_c \leq \alpha <\sim 70°$, the shear layer is thicker and shifted further away from the cylinder surface. The maximum u' (0.18-0.2**U**) changes little with $\alpha$, indicating that turbulent transition has occurred. Its peak location remains close to the shear layer mid-point: $y' \equiv u/(u_{max}-u_{min}) = 0.5$. On the unperturbed side, the u and u' profiles appear unaffected by changes on the wire side, The maximum u' has a similar magnitude and changes little with wire position.

The influence of $\alpha$ on the shear layer thickness and displacement is compactly summarized in Fig. 10 in terms of the vorticy thickness: $\Lambda \equiv (u_{max} - u_{min}) \Big/ \left(\frac{\partial u}{\partial y}\right)_{max}$ and y', respectively. Generally, the boundary layer is not affected on the unperturbed side, while on the wire side the shear layer is thicker and further from the cylinder in the range when final separation occurs at the tripwire. A reduction in y' is observed when Xr is reduced, while $\Lambda$ changes little.

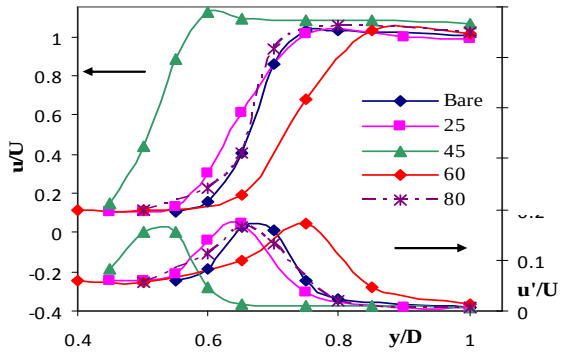


Figure 9. u/**U** and u'/**U** Shear layer profiles at $x/D = 0.5$, $z/H = 0.25$ for AR = 6.

Closer inspection of the v' field for AR = 6, $\alpha = 55°$ indicates a very rapid adjustment of the shear layer position in the region $x/D < 1$, which can be attributed to the intense mixing in the base region induced partly by the vortex formation process and increased thickness. Despite the differences in the separation point (and resulting shift y': Fig. 9,10), the shear layer intensity remains similar, suggesting that the circulation flow to the forming vortices is similar on both sides of the cylinder. Hence, the shed vortices are expected to be of roughly equal strength, as corroborated by the similarity of the fluctuation spectra on opposing sides of the wake, which promotes symmetry of the wake velocity field.

The *rms* of the lateral velocity, v', are shown in Fig. 11a along the line $y = 0$, $z = 0.3H$. For AR = 3, the evolution is similar for all AR, but the maximum is reached earlier for $\alpha = 55°$ ($<\alpha_c$), which is consistent with the observed reduction of Xr since the maximum v' indicates the end of the formation region and is generally located in the immediate vicinity of the end of the mean recirculation region (Cantwell and Coles, 1983). For AR = 6, the location of the peak v' also correlates with Xr. However, unlike for AR = 3, the magnitude of v' changes dramatically as a function of $\alpha$. Lateral profiles at $x =$ Xr ($z/H = 0.3$) are compared in Fig. 11b,c. In general, for $\alpha > \alpha_c$, the profiles are symmetric and similar to the bare cylinder case. For $\alpha = 55°$ ($<\alpha_c$), the distributions suggest a narrower wake, consistent y' and Xr in Fig. 6 and 10, and a slight asymmetry towards the unperturbed side ($y > 0$). Whereas for AR = 3 the u' and v' levels remain comparable for all $\alpha$, for AR = 6 the v' levels are significantly larger for $\alpha = 55°$ even though the u' levels change little, consistent with stronger shed vortices. The vertical distribution of w' and w (Fig. 12) shows that the maximum of w' coincides with a local minimum in w-magnitude, effectively separating tip flow from the wake recirculation. For all values of $\alpha$, spectra of the velocity fluctuations at downstream locations show that for elevations higher than that for w'- maximum, the peak associated with $f_s$ is difficult to discern in comparison to lower elevations ($z < 0.6H$). This region of elevated w' arises from the interference between the flapping shear layer from the free-end and the vortex formation process at lower elevations.

## CONCLUDING REMARKS

The aforementioned results suggest that an asymmetrically placed tripwire affects the shedding process and wake structure through a delay in the surface boundary layer separation. The influence of the aspect ratio on the tripwire effectiveness is a result of the tip flow interference as evidenced by the location of the maximum w'. For sub-critical $\alpha$, a combination of tripwire triggered separation and thicker shear layer appears to concentrate vortex formation activity and reduce three-dimensional effects.

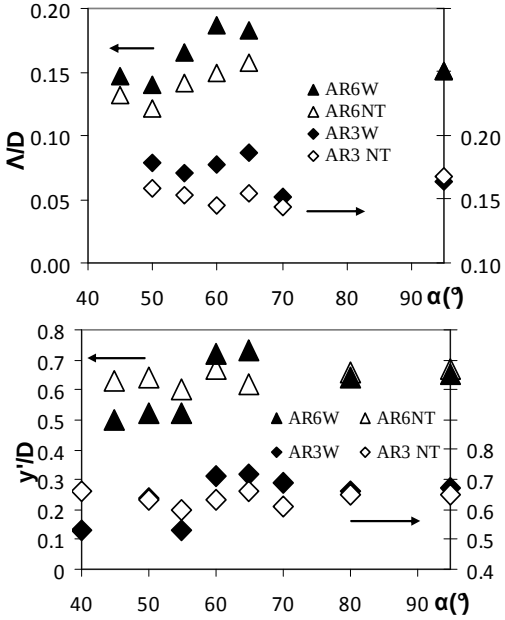


Figure 10. Vorticity thickness Λ and shear layer displacement versus α. Symbols on right margin indicate bare cylinder case.

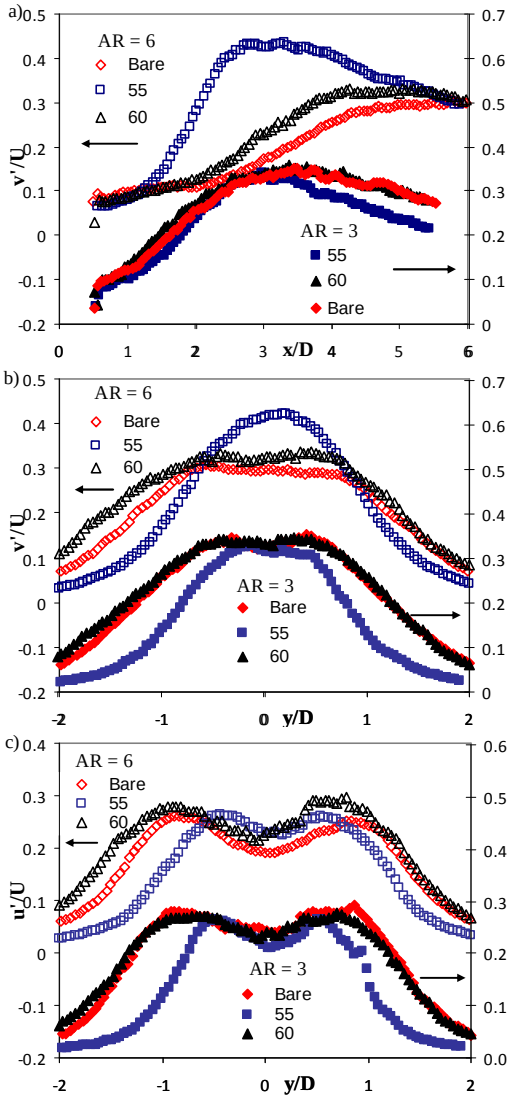


Figure 11. Velocity rms for AR = 3 and AR = 6 in the plane $z/H = 0.3$: a) v' vs $x/D$; b) v' vs $y/D$ and c) u' vs $y/D$.

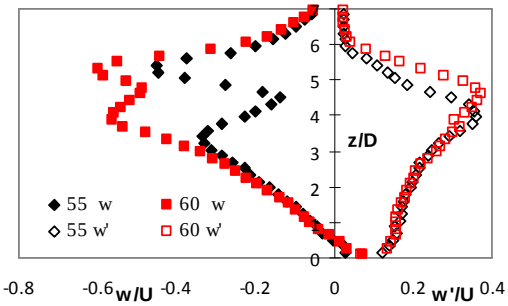


Figure 12. Distribution of w and w' along $y = 0$ for AR = 6.

## REFERENCES


Cantwell, B., Coles, D., 1983, "An experimental study of entrainment and transport in the turbulent wake of a circular cylinder," *J. Fluid Mech.* 136, 321-374.

Ekmekci, A, Rockwell, D., 2010, "Effects of a geometrical disturbance on flow past a circular cylinder: a large-scale spanwise wire," *J. Fluid Mech.* 665, 120-157.

Igarashi, T, 1986, "Effect of tripping wires on the flow around a circular cylinder normal to an airstream," *Bull. Jpn. Soc. Mech. Eng.*, 29, 2917-2924.

Mahbub Alam, Md., Zhou, Y., Zhao, J.M., Flamand, O., Boujard, O., 2010, "Classification of tripped cylinder wake and bi-stable phenomenon," *Int. J. Heat and Fluid Flow*, 31, 545-560.

Nebres, J., Batill, S., 1993, "Flow about a circular cylinder with a single large-scale surface perturbation," *Exp. in Fluids*, 15, 369-379

Ruiz, T., C. Sicot, L.E. Brizzi, J. Laumonier, J. Borée, and Y. Gervais, 2009, "Unsteady near wake of a flat disk normal to a wall," *Exp in Fluids*, 47-4/5: p. 637-654